Available online at www.sciencedirect.com
ScienceDirect
Journal of Power Sources 160 (2006) 1104–1110
JOURNAL OF POWER SOURCES
www.elsevier.com/locate/jpowsour

Evaluation of Ni–Cr-base alloys for SOFC interconnect applications

Zhenguo Yang *, Guan-Guang Xia, Jeffry W. Stevenson

Pacific Northwest National Laboratory, Richland, WA 99352, United States

Received 4 January 2006; received in revised form 24 February 2006; accepted 27 February 2006
Available online 8 May 2006

Abstract

To further understand the suitability of Ni–Cr-base alloys for solid oxide fuel cell (SOFC) interconnect applications, three commercial Ni–Cr-base alloys, Haynes 230, Hastelloy S and Haynes 242 were selected and evaluated for oxidation behavior under different exposure conditions, scale conductivity and thermal expansion. Haynes 230 and Hastelloy S, which have a relatively high Cr content, formed a thin scale mainly comprised of Cr_2O_3 and $(Mn,Cr,Ni)_3O_4$ spinels under SOFC operating conditions, demonstrating excellent oxidation resistance and a high scale electrical conductivity. In contrast, a thick double-layer scale with a NiO outer layer above a chromia-rich substrate was grown on Haynes 242 in moist air or at the air side of dual exposure samples, indicating limited oxidation resistance for the interconnect application. With a face-centered-cubic (FCC) substrate, all three alloys possess a coefficient of thermal expansion (CTE) that is higher than that of candidate ferritic stainless steels, e.g. Crofer22 APU. Among the three alloys, Haynes 242, which is heavily alloyed with W and Mo and contains a low Cr content, demonstrated the lowest average CTE at $13.1 \times 10^{-6}\,K^{-1}$ from room temperature to 800 °C, but it was also observed that the CTE behavior of Haynes 242 was very non-linear.

Keywords: Solid oxide fuel cell; Interconnect; High temperature alloys; Oxidation

1. Introduction

Over the past years, advances in materials and cell fabrication technology have led to a steady reduction in SOFC operating temperatures to the intermediate range of 650–800 °C. Consequently it has become possible to consider high temperature oxidation-resistant alloys as the stack interconnect materials, instead of lanthanum chromites [1–5]. Compared to doped lanthanum chromites, alloys offer several advantages, including significantly lower raw material and fabrication costs. However, the SOFC operating conditions present significant challenges for alloy-based interconnects, as the interconnects are exposed simultaneously to an oxidant gas (air) at the cathode side and a reducing gas (e.g. H_2) at the anode side during operation.

At high temperatures, oxidation-resistant alloys rely on thermal growth of an oxide scale on their surfaces to protect the metal substrates from further environmental attack. In terms of composition, the scale can be either a semi-conducting chromia layer, or an electrically insulating alumina or silica layer, depending on the concentration of the scale forming elements in the metal substrate. Only the chromia-forming alloys are generally considered for interconnect applications, as low electrical resistivity is required to minimize ohmic losses within the stacks. Among the chromia-forming oxidation-resistant alloys, the body-centered-cubic (BCC) ferritic stainless steels (FSS) demonstrate good oxidation resistance and the ability to match the coefficient of thermal expansion (CTE) of adjacent cell/stack components [6–10]. However, FSS face several challenges including long-term surface stability, increasing electrical resistance due to scale growth during prolonged stack operation, and low high temperature mechanical strength. In comparison, the face-centered-cubic (FCC) Ni–Cr- or Ni–Fe–Cr-base alloys (or in particular superalloys) are generally much stronger and more oxidation resistant (i.e. lower scale growth rate) in the SOFC interconnect operating environment [8,11–13]. However, the FCC Ni-base alloys with sufficient Cr to provide oxidation resistance often exhibit a high CTE, typically in the range of $15.0–20.0 \times 10^{-6}\,K^{-1}$ from room temperature to 800 °C [7,8]. There are Ni-base alloys with lower CTE, notably the Invar type Ni–Fe-base (~64% Fe) alloys and some Ni–W–Mo–Cr-base compositions [14–16]. To obtain a relatively low CTE, these alloys must contain low (or zero) levels of chromium, and therefore may not

* Corresponding author. Tel.: +1 509 375 3756; fax: +1 509 375 2186.
E-mail address: zgary.yang@pnl.gov (Z. Yang).

0378-7753/$ – see front matter © 2006 Elsevier B.V. All rights reserved.
doi:10.1016/j.jpowsour.2006.02.099

Table 1
Chemical compositions of Ni–Cr-base alloys

Alloys	Nominal composition (wt.%)											
	Ni	Cr	Fe	Co	C	Mn	Si	Mo	W	Al	B	Others
Haynes 230[a]	Bal	22.0	3.0[b]	5.0[b]	0.10[b]	0.5	0.4	2.0	14.0	0.30	0.015[b]	0.5Cu[b]
Hastelloy S[a]	Bal	16.0	3.0[b]	2.0[b]	0.02[b]	0.5	0.4	15.0	1.0[b]	0.25	0.015[b]	0.02La
Haynes 242[a]	Bal	12.0	2.0[b]	2.5[b]	0.03[b]	0.8[b]	0.8[b]	25.0	–	0.5[b]	0.015[b]	

[a] Haynes 230, Hastelloy S and Haynes 242 are registered trademarks of Haynes International.
[b] m, maximum.

exhibit sufficient oxidation resistance for SOFC interconnect applications.

Even with a relatively high CTE, the Ni–Cr-base alloys could find application as interconnect materials through the use of innovative SOFC stack and seal designs and/or novel interconnect structures. For example, recent proof-of-concept work has confirmed the potential viability of a cladding approach to fabricate a stable composite interconnect structure consisting of the FCC Ni–Cr-base alloy claddings over a BCC ferritic stainless steel substrate [17]. The cladding approach not only potentially helps solve the high CTE issue of Ni–Cr-base alloys, but can also offset the higher cost of the Ni–Cr-base alloys compared to FSS compositions. Thus, there is a need to further understand the behavior of Ni-base alloys and to identify suitable compositions to provide another option for SOFC developers in their efforts to design and fabricate stable metallic interconnects. With this regard, three commercial Ni–Cr-base alloys-containing different Cr contents were selected and evaluated against properties relevant for SOFC interconnection applications.

2. Experimental

Three commercial alloys were studied: Haynes 230, Hastelloy S, and Haynes 242 [18–20]. The alloys were provided in the form of 1.0 mm thick sheets by Haynes International Inc. in Kokomo, Indiana. The alloy compositions are listed in Table 1. About 25.4 mm × 12.7 mm coupons were cut from the sheet stock and polished with 600 grid SiC sand papers.

The alloys were evaluated via isothermal oxidation tests in moist air, moist hydrogen, and dual exposure conditions typical of SOFC interconnects, i.e. they were exposed simultaneously to moist air at one side and moist hydrogen at the other side. The isothermal oxidation testing in air was performed by suspending polished, cleaned coupons from an alumina rod in a tube furnace. The coupons were heated to 800 °C at 5 °C min^{-1}, held at this temperature for 300 h, and then cooled to room temperature. A steady flow of moist air (~3% H_2O was introduced by flowing the air through a room temperature water bubbler) was maintained throughout the oxidation tests. The oxidized coupons were then weighed prior to structure and microstructure characterization. The study on oxidation behavior of the Ni-base alloys in moist hydrogen and under dual exposure conditions was carried out in a specifically designed apparatus described in previous publications [21,22]. The dual atmosphere specimen was prepared by sealing a 25.0 mm diameter circular disk of a selected alloy to the end of an E-brite tube using BNi-2 braze. After verification of hermetic sealing by a helium leak test, the E-brite tube and the alloy disk were placed in the test-stand, along with a coupon which was exposed to moist hydrogen only. After the test, the sample was removed by cutting out the inner area of the circular disk, and then ultrasonicated in acetone for 5 min.

XRD analysis on the oxidized alloy coupons was performed using a Philips XRG-3100 X-ray Generator with Cu Kα radiation. SEM analysis was performed using a JEOL scanning electron microscope (model 5900LV) equipped with energy-dispersive spectroscopic (EDS) capability at an operating voltage of 20 kV. After surface analysis, the coupons were epoxy-mounted, sectioned, polished, and further examined under the SEM. The coupons from the electrical resistance measurements (described below) were also sectioned and analyzed under the SEM.

The electrical resistance of the scales was measured using a four-probe dc technique. Details of the test arrangement can be found in a previous publication [10]. Before the tests, Pt contact paste was applied between two symmetrical alloy coupons and Pt wires were spot-welded to the coupons. To avoid interdiffusion between the alloys and Pt paste, the alloy coupons were preoxidized in air at 800 °C for 100 h prior to the application of the Pt paste. After heating the samples to 800 °C, a constant current density of 500 mA cm^{-2} was applied to the coupons through two Pt leads, while the voltage drop across the interfaces between the two alloy coupons was measured with the other two Pt leads. The area specific resistance (ASR, expressed in Ω cm^2) of the scales was then calculated according to Ohm's Law, ASR = $V/2i$, where V is the voltage drop and i is the current density. The factor of 2 was included to account for the fact that the voltage drop was measured across two scales connected in series.

The CTE of the selected Ni–Cr-base alloys was determined with a Linseis L75 dual push-rod dilatometer.

3. Results and discussion

3.1. Oxidation, scale composition and structure

Fig. 1 shows the XRD results on the alloy samples after oxidation, indicating that the scales grown on these alloys were comprised of Cr_2O_3 and M_3O_4 (M = Mn, Ni, Cr) spinel, as well as NiO for Haynes 242 and Hastelloy S. Cr_2O_3 appeared to be the dominant component in the scale grown on Haynes 230, which contains the highest Cr content among the three. In contrast, NiO became a major phases in the scale grown on Haynes 242, which has the lowest Cr content. Due to penetration of X-rays

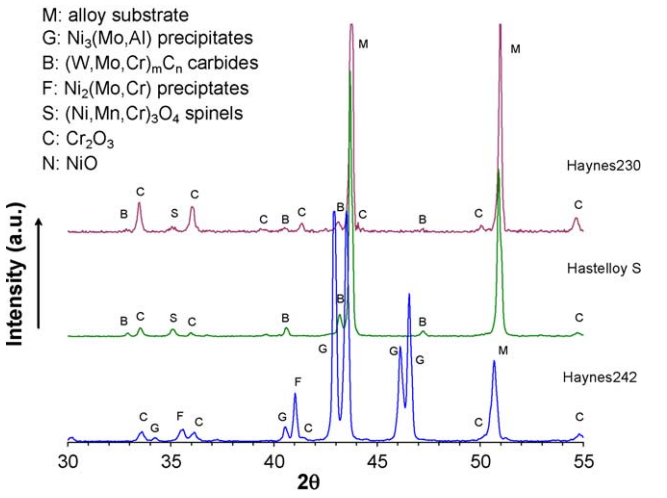

Fig. 1. Surface X-ray diffraction patterns of Haynes 230, Hastelloy S and Haynes 242 alloys after isothermal oxidation in moist air (3% H_2O) at 800 °C for 300 h.

through the scales or scale chipping (observed on Haynes 242), diffraction peaks of the FCC metal substrate and second phases or precipitates in the alloy are also visible in the patterns. Fig. 2 shows SEM cross-sections of the three selected alloys after the oxidation. The scale grown on Haynes 242 was much thicker than the other two, and demonstrated a double-layer structure with a NiO layer atop a chromia-rich sub-layer. Cracks were observed at the interface of the double layers. In comparison, only a thin scale was grown on Haynes 230 or Hastelloy S, and the scales appeared to be well-bonded to the metal substrates. EDS point analysis on the scales grown on these two alloys revealed a substantial amount of Mn in the scales, indicating formation of Mn-containing spinels during the high temperature exposure. Thus, similar to ferritic compositions [6,10], residual Mn or the addition of a small amount of Mn into Ni–Cr-base alloys can lead to formation of Mn-containing spinels in the scales grown on the alloys during high temperature exposures. The spinel formation in the scale grown on Haynes 230 was also confirmed by previously published works [11,12,23]. Also, the EDS analysis revealed a small amount of NiO in the scale grown on Hastelloy S, while no noticeable NiO was found in the scale on Haynes 230.

Overall it appears that, due to the presence of sufficient Cr in the metal substrate, Haynes 230 and Hastelloy S formed a thin scale that was dominated with Cr_2O_3 and spinels, and thus demonstrated excellent oxidation resistance in moist air. In contrast, a thick, defective double-layer scale was grown on Haynes 242, which contains only 8% Cr, raising concern over its oxidation resistance for SOFC interconnect applications.

3.2. Oxidation behavior in air, hydrogen, and dual atmospheres

To further examine and understand their oxidation resistance under SOFC operating conditions, the selected alloys were further tested in moist hydrogen and in moist air-moist hydrogen dual atmospheres. Fig. 3 shows XRD patterns from the alloy samples after 300 h oxidation at 800 °C in moist hydrogen. The

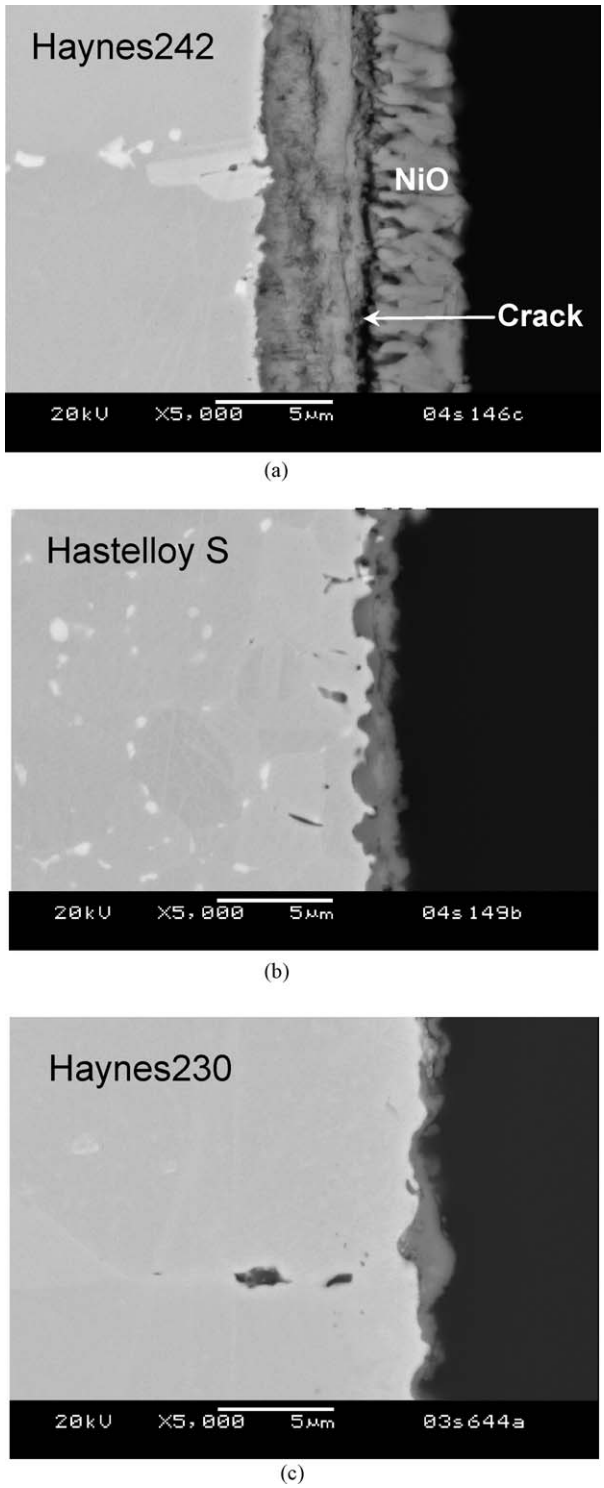

Fig. 2. SEM cross-sections of Haynes 242, Hastelloy S and Haynes 230 alloys after oxidation at 800 °C in moist air (3% H_2O) for 300 h.

XRD analysis indicates that the scales grown on these three alloys were mainly of Cr_2O_3 and M_3O_4 (M = Mn, Ni, Cr) spinel, but not NiO. This is not surprising, since formation of NiO is thermodynamically unfavorable in the moist hydrogen environment. Again, due to penetration of X-ray through the scales, the γ-metal substrate and other phases in the substrate are visible in the patterns. SEM analysis on the cross-sections of the oxidized

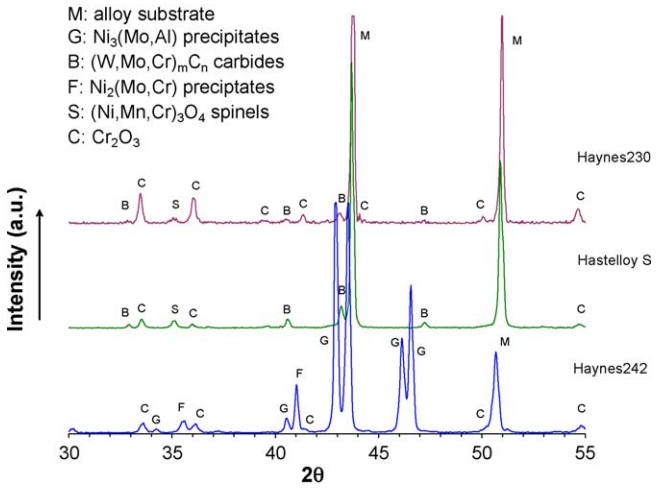

Fig. 3. Surface X-ray diffraction patterns of Haynes 230, Hastelloy S and Haynes 242 alloys after isothermal oxidation in moist hydrogen (3% H_2O) at 800 °C for 300 h.

samples, as shown in Fig. 4, found a similar thickness of scales grown on these three alloys; all scales were well-bonded to the metal substrates. Thus, all three alloys demonstrated an excellent oxidation resistance in the moist hydrogen environment, independent of Cr content in the metal substrate.

Similar oxidation behavior at 800 °C was observed on the moist hydrogen side of samples that were simultaneously exposed to moist air on the other side during dual atmosphere oxidation tests. However, a difference in oxidation behavior was observed between the air side of the dual exposure samples (shown in Fig. 5) and the samples that were exposed to moist air at both sides (refer back to Fig. 2). For example, while the scale that grew on Hastelloy S in moist air only contained a small amount of NiO, no NiO was detected in the scale grown on the air side of the dual exposure sample. The suppression of the formation of NiO at the air side under the dual exposure was however not that drastic for Haynes 242. As shown in Fig. 5(b), the scale grown on the air side of Haynes 242 during the dual exposure showed a similar dual-layer structure to the scale grown in moist air only, though it was slightly thinner, and cracks were clearly noticeable at the interface between the top NiO layer and the spinel-rich sub-layer. In addition, the interfaces between the scales and the metal substrates at the air side of the dual exposure samples appeared to be free from defects such as porosity, which was observable along the scale and metal substrate interfaces of samples exposed to air only. This phenomenon was not observed however on Hastelloy S, due to the buckling of scale grown at the air side during the dual exposure.

In short, the dual atmosphere exposure led to a different oxidation behavior of the Ni-base alloys at the air side of dual exposure samples, in comparison with the samples exposed to moist air at both sides. Similarly, an anomalous oxidation behavior was also observed on ferritic stainless steels at the airside of dual exposure samples [21,22]. In comparison, however, for ferritic stainless steels the dual exposures often led to growth of hematite nodules and localized attack. The anomalous oxidation behavior of varied alloys under the dual exposures is tentatively

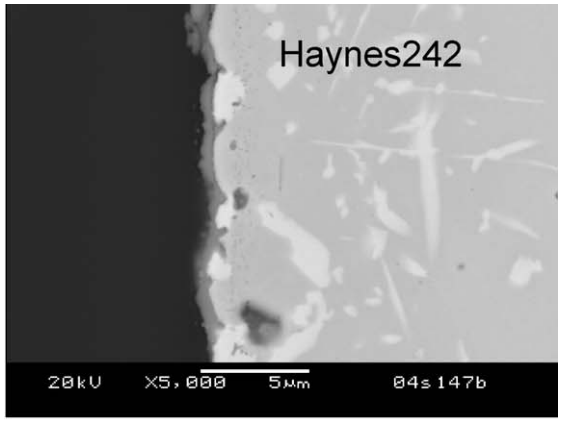

(a)

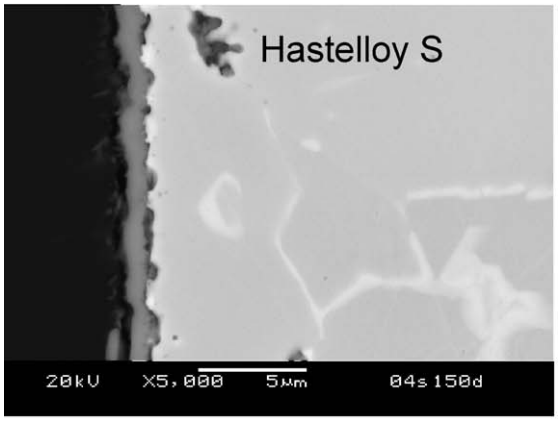

(b)

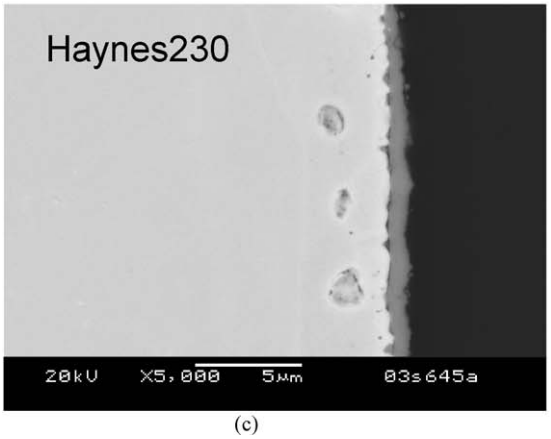

(c)

Fig. 4. SEM cross-section of: (a) Haynes 242, (b) Hastelloy S, and (c) Haynes 230 alloys after oxidation at 800 °C in moist hydrogen (97% H_2 + 3% H_2O) for 300 h.

attributed to a hydrogen flux through the alloys from the fuel side to the air side and the subsequent presence of hydrogen or protons at the air side, which likely alters the scale structure and growth.

3.3. Scale electrical conductivity

As a bi-polar plate between adjacent cells, the interconnect must offer a low resistance electrical path in order to mini-

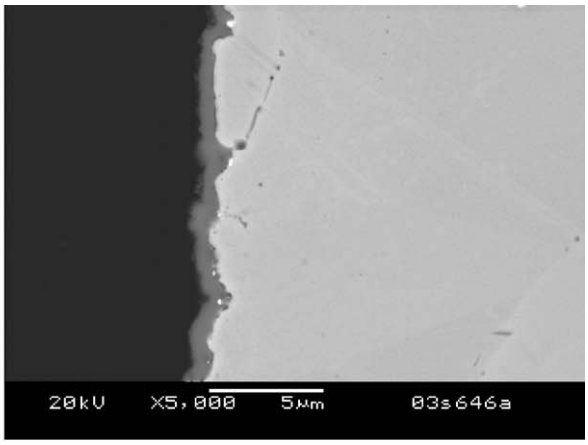

(a)

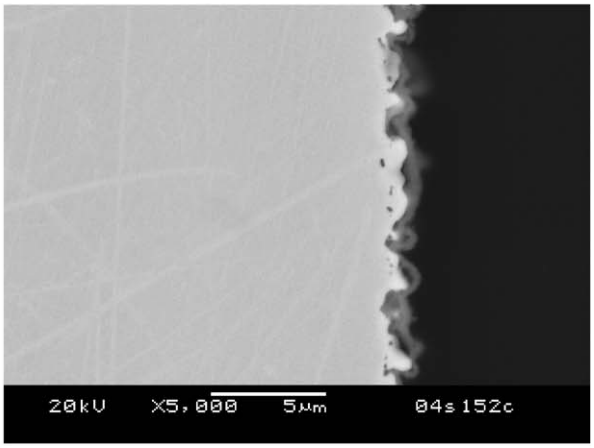

(b)

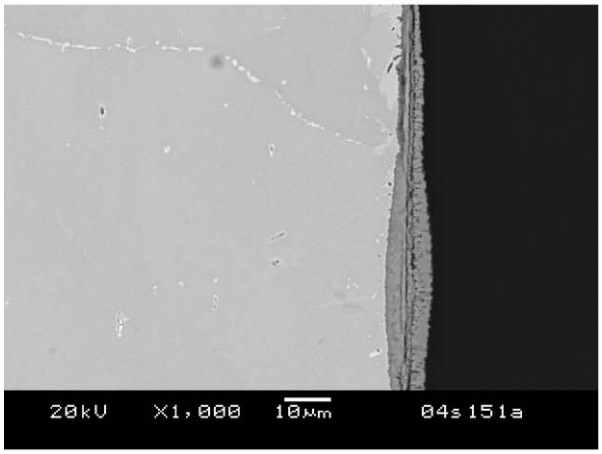

(c)

Fig. 5. SEM cross-sections at air side of Ni–Cr-base alloys after oxidation at 800 °C for 300 h under dual atmosphere exposure, i.e. with moist air (air + 3% H_2O) at one side (air side) and moist hydrogen (H_2 + 3% H_2O) at the other (hydrogen side): (a) Haynes 230, (b) Hastelloy S, and (c) Haynes 242.

mize resistive losses within SOFC stacks. For oxidation-resistant alloys, the electrical resistance is the sum of two parts, bulk alloy resistance and scale resistance. For high temperature applications such as the SOFC interconnect, the electrical resistance of the scale usually dominates the electrical behavior of the

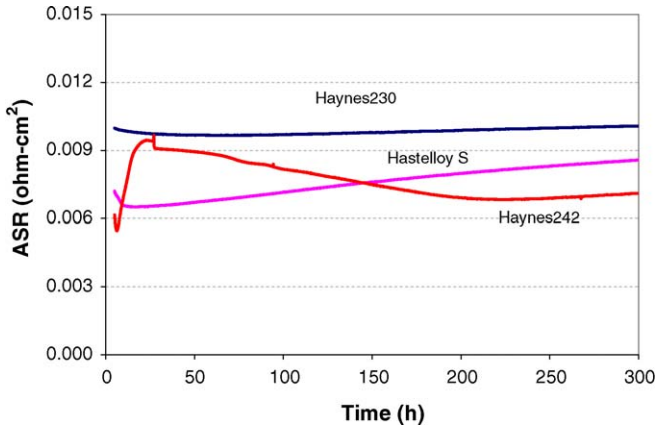

Fig. 6. Area specific resistance (ASR) of Haynes 230, Hastelloy S, and Haynes 242, as a function of time during isothermal oxidation in air at 800 °C. The test coupons were pre-oxidized for 100 h at 800 °C in air before the ASR measurement.

oxidation-resistant alloys. The measured electrical conductivity of the selected Ni–Cr-base alloys (including their scales) as a function of time at 800 °C in air is shown in Fig. 6. Among the three alloys, Haynes 230 exhibited a higher ASR that nevertheless only increased slightly over time due to its slow scale growth. In comparison, Hastelloy S showed a lower ASR in the early stages, but its ASR increased more quickly than that of Haynes 230 due to its higher scale growth rate. For Haynes 242, its ASR appeared to increase drastically in early stages, then dropped slowly over the time and eventually leveled off. It is noted that there is a spike on the ASR curve of Haynes 242, which was likely caused by a power failure occurring during the test.

Overall the three Ni–Cr-base alloys demonstrated a scale conductivity that was higher than many commercial ferritic stainless steels, and comparable to that of the newly developed stainless steel Crofer22 APU [6,10]. In the long term, however, the high rate of scale growth, and defective nature of the scale, might lead to excessively high ASR for Haynes 242, especially for SOFC applications requiring numerous thermal cycles.

3.4. Thermal expansion

Fig. 7 shows the thermal expansion behavior of the selected Ni–Cr-base alloys as a function of temperature. As expected, with a FCC matrix the selected Ni–Cr-base alloys demonstrate a higher CTE than the BCC ferritic stainless steels, which typically have a CTE of 12.0–13.0 × 10^{-6} K^{-1}. Among the three alloys, Haynes 230 has the highest CTE at 14.9 × 10^{-6} K^{-1} from room temperature to 800 °C, which is similar to that of Hastelloy S at 14.8 × 10^{-6} K^{-1}, but much higher than that of Haynes 242 at 13.1 × 10^{-6} K^{-1}. It is clear that, to some extent, the CTE of Ni–Cr-base alloys can be modified through alloying. Previous work [14,15] indicated that Cr additions increased the CTE of the Ni–Cr substrate, while Mo, W, Al and Ti decreased the CTE. Thus, the relatively low CTE of Haynes 242 can be attributed to extensive additions of W and Mo, and the limited amount of Cr. The heavy alloying with refractory metal

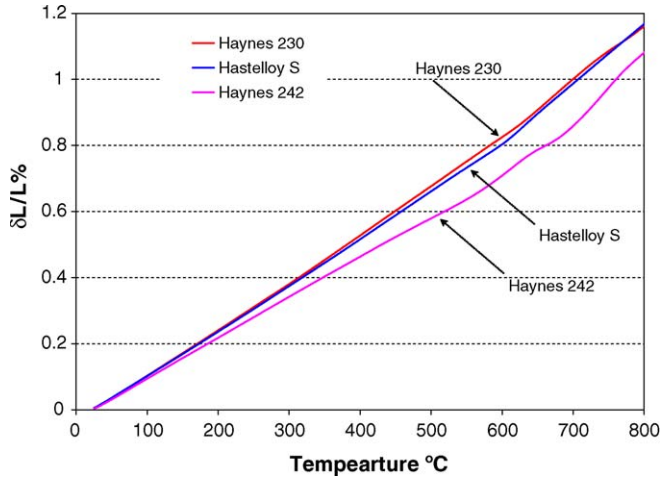

Fig. 7. Thermal expansion of Haynes 230, Hastelloy S and Haynes 242.

elements, however, results in non-linearity of the CTE; also, the relatively low Cr content can potentially lead to a reduced oxidation-resistance that can be insufficient for SOFC interconnect applications.

4. Summary and conclusions

As has been observed, Haynes 230 and Hastelloy S, which have a relatively high Cr content, formed a thin scale mainly comprised of Cr_2O_3 and $(Mn,Cr,Ni)_3O_4$ spinel during high temperature exposure in moist air; this scale provided excellent oxidation resistance. On the other hand, Haynes 242 developed a thick double-layer scale consisting of a NiO outside layer above a chromia-rich substrate, raising concern over its oxidation resistance for the interconnect applications. All three alloys exhibited excellent oxidation resistance in moist hydrogen, growing a thin scale that was dominated with Cr_2O_3 and $(Mn,Cr,Ni)_3O_4$ spinels for Haynes 230 and Hastelloy S, and with Cr_2O_3 as for Haynes 242. Similarly, a thin scale consisting of Cr_2O_3 the major phase also developed on all three alloys at the moist hydrogen side when they were exposed to a dual atmosphere (moist air versus moist hydrogen) environment. Somewhat different oxidation behavior was, however, observed at the air side of the dual atmosphere samples compared to samples exposed to moist air at both sides. In particular, it appeared that hydrogen flux from the fuel side to the air side tended to mitigate formation of NiO and reduce porosity along the scale/metal interfaces. However, the dual atmosphere exposure did not significantly alter the oxidation behavior of Haynes 242, which still formed a thick, defective, double-layer scale on its surface.

Due to the formation of Mn-containing spinels in their surface scales and their excellent oxidation resistance, both Haynes 230 and Hastelloy S demonstrated an ASR that was comparable to that of Crofer22 APU. The poor stability of the scale on Haynes 242 would likely result in an unacceptably high scale ASR during typical SOFC stack operating lifetimes.

With a FCC substrate, all three alloys exhibited a CTE that is higher than that of candidate ferritic stainless steels, e.g. Crofer22 APU. Among the three alloys, Haynes 242, which is heavily alloyed with W and Mo and has a low Cr content, demonstrated the lowest average CTE ($13.1 \times 10^{-6}\,K^{-1}$) from room temperature to 800 °C. The reduction in CTE via alloying, however, resulted in limited oxidation resistance, as well as a decreased linearity in the alloy CTE.

To sum up, the Ni–Cr-base alloys, which are mechanically stronger than ferritic stainless steels, also demonstrate excellent oxidation resistance and satisfactory scale electrical conductivity for SOFC interconnect applications if they contain enough Cr. To fully make use of the advantages of the Ni-base alloys, however, novel designs of interconnects or stacks are needed to address potential CTE mismatch to cell components. Though the high CTE of Ni-base alloys can to some extent be modified via alloying, attention must be paid to the effects of compositional changes on their oxidation resistance and other properties such as CTE linearity.

Acknowledgements

The authors would like to thank Nat Saenz, Shelly Carlson, and Jim Coleman for their assistance in metallographic and SEM sample preparation and analysis. The work summarized in this paper was funded as part of the Solid-State Energy Conversion Alliance (SECA) Core Technology Program by the U.S. Department of Energy's National Energy Technology Laboratory (NETL). The authors would like to acknowledge helpful discussions with Wayne Surdoval, Lane Wilson, Don Collins, and Travis Schulz. PNNL is operated by Battelle Memorial Institute for the U.S. Department of Energy under Contract DE-AC06-76RLO 1830.

References

[1] N.Q. Minh, T. Takahashi, Science and Technology of Ceramic Fuel Cells, Elsevier, New York, 1995.
[2] B.H. Steele, Nature 414 (2001) 345.
[3] M. Dokiya, Solid State Ionics 152–153 (2002) 383.
[4] H.U. Anderson, F. Tietz, in: S.C. Singhal, K. Kendall (Eds.), High Temperature SOFCs: Fundamentals, Design and Applications, Elsevier Advanced Technology, Oxford, 2003, p. 173.
[5] S.P.S. Badwal, R. Bolden, K. Foger, in: P. Stevens (Ed.), Proceedings of the Third Eur. SOFC Forum, European Solid Oxide Fuel Cell Forum, Switzerland, 1998, p. 105.
[6] W.J. Quaddakkers, J. Piron-Abellan, V. Shemet, L. Singheiser, Mater. High Temp. 20 (2003) 115.
[7] J.W. Fergus, Mater. Sci. Eng. A 397 (2005) 271.
[8] Z. Yang, K.S. Weil, D.M. Paxton, J.W. Stevenson, J. Electrochem. Soc. 150 (2003) A1188.
[9] W.Z. Zhu, S.C. Deevi, Mater. Sci. Eng. A 348 (2003) 227.
[10] Z. Yang, J.S. Hardy, M.S. Walker, G. Xia, S.P. Simner, J.W. Stevenson, J. Electrochem. Soc. 151 (2004) A1825.
[11] D.M. England, A.V. Virkar, J. Electrochem. Soc. 146 (1999) 3196.
[12] D.M. England, A.V. Virkar, J. Electrochem. Soc. 148 (2001) A330.
[13] C.T. Sims, N.S. Stoloff, W.C. Hagel (Eds.), Superalloys II, John Wiley & Sons, Inc., NY, 1987.
[14] R. Yamamoto, Y. Kadoya, H. Kawai, R. Magoshi, T. Noda, S. Tamano, S. Ueta, S. Isobe, Schriften des Forschungszentrums Juelich, Reihe Energietechnik. Part 3. Materials for Advanced Power Engineering 21 (2002) 1351.

[15] D.E. Alman, P.D. Jablonski, in: K.A. Green, T.M. Pollock, H. Harada, T.E. Howson, R.C. Reed, J.J. Schirra, S. Walston (Eds.), Superalloys 2004, TMS, Warrendale, PA, 2004, p. 617.
[16] G.R. Holcomb, D.E. Alman, J. Mater. Eng. Perform., in press.
[17] L. Chen, Z. Yang, B. Jha, G. Xia, J.W. Stevenson, J. Power Sources 152 (2005) 40.
[18] D.L. Klarstrom, US Patent 4,476,091 (1984).
[19] D.S. Acuncius, et al., US Patent 3,418,111 (1968).
[20] M.K. Miller, I.M. Anderson, L.M. Pike, D.L. Klarstrom, Mater. Sci. Eng. A 327 (2002) 89.
[21] Z. Yang, M.S. Walker, P. Singh, J.W. Stevenson, Electrochem. Solid State Lett. 6 (2003) B35.
[22] Z. Yang, G. Xia, P. Singh, J.W. Stevenson, Solid State Ionics 176 (2005) 1495.
[23] J. Li, J. Pu, J. Xiao, X. Qian, J. Power Sources 139 (2005) 182.